AFRL-VS-HA-TR-2006-1028

ARTICLE IN PRESS

ELSEVIER

Journal of Atmospheric and Solar-Terrestrial Physics ▮ (▮▮▮▮) ▮▮▮–▮▮▮

Journal of ATMOSPHERIC AND SOLAR-TERRESTRIAL PHYSICS

www.elsevier.com/locate/jastp

DTIC COPY

A potential remote-sensing technique for thermospheric temperature with ground-based resonant atomic oxygen Raman lidar

Ramesh D. Sharma*, Phan D. Dao

Air Force Research Laboratory, Space Vehicles Directorate/VSBY, Hanscom AFB, MA 01731, USA

Received 19 May 2005; received in revised form 13 September 2005; accepted 1 October 2005

Abstract

We propose a remote-sensing technique to measure temperature in the lower thermosphere with a resonant Raman lidar. A ground-based pulsed laser operating at 630.0304 (636.3776) nm excites $^3P_2$ ($^3P_1$) multiplet level of the ground electronic state of atomic oxygen in the atmosphere to the electronically excited $^1D_2$ state and the back-scattered photons at 636.3776 (630.0304) nm, while the atom transitions to $^3P_1$ ($^3P_2$), are detected. Using the backscattering Raman cross sections calculated here we show: (1) For the range of altitudes in the lower thermosphere where the fine-structure multiplets of atomic oxygen are in thermodynamic equilibrium with the local translational temperature (LTE) and the electronically excited intermediate state $^1D_2$ remains relaxed primarily by collisions with N_2 and O_2, the ratio of the backscattered signal can be used to obtain temperature. (2) Higher up, for the range of altitudes where the fine-structure multiplets of atomic oxygen are in LTE and the electronically excited intermediate state $^1D_2$ is relaxed primarily by spontaneous emission of a photon, the Stokes and anti-Stokes backscattered signal can be used to obtain the atomic oxygen density and local temperature. (3) Still higher up, for the range of altitudes where the fine-structure multiplets of atomic oxygen are not in LTE and the electronically excited intermediate state $^1D_2$ is relaxed primarily by spontaneous emission of a photon, the Stokes and anti-Stokes backscattered signal can be used to obtain the density of the $^3P_2$ and $^3P_1$ multiplet levels of the ground electronic state of atomic oxygen. For a ground-based instrument a simulation with 3 km range gate is used to show that the relative error of temperature measurements from 100 to 250 km could be less than 30%. It is pointed out that this technique has the potential of providing unique data that addresses the modeling of satellite drag and the effects of space weather on the upper atmosphere. In addition, this technique may also permit the detection of the thickness of the temperature inversion layers as well as their temperature and density perturbations.
© 2005 Elsevier Ltd. All rights reserved.

Keywords: Middle and upper atmosphere; Atomic oxygen density; Temperature; Resonant Raman scattering; Remote sensing

20060214 000

1. Introduction

The upper middle atmosphere and the lower thermosphere contain at the lower boundary the coldest part of the atmosphere and at the upper boundary abrupt transition to the higher temperatures of the thermosphere. The steep rise in

*Corresponding author. Tel.: +1 781 3774198.
E-mail address: ramesh.sharma@hanscom.af.mil (R.D. Sharma).

1364-6826/$ - see front matter © 2005 Elsevier Ltd. All rights reserved.
doi:10.1016/j.jastp.2005.10.001

DISTRIBUTION STATEMENT A
Approved for Public Release
Distribution Unlimited

temperature is accompanied by many interesting chemical and dynamical effects. Prominent among the chemical effects is the steep rise in the atomic oxygen density and its dominant role in cooling the atmosphere (Sharma and Roble, 2001, 2002). Prominent among the dynamical effects is the breaking of gravity waves and energy deposition in the mesosphere and lower thermosphere leading to large perturbations in temperature and density. Existing range-resolved remote-sensing techniques for diagnostics of temperature and density in the mesosphere are based on lidar, operating on metal atom transitions, dependent on the backscattered radiation from meteoric metal layers (Na (Gardner, 1989), K (von Zahn and Hoffner, 1996), and Fe (Gelbwachs, 1994)). Although these lidar techniques are confined to below 120 km, they provide a wealth of information on temperature, winds and density perturbations. The technique proposed in this paper addresses the critical gap of range-resolved temperature data in the region above that limit. At those altitudes, there are a number of resonance scattering lidar techniques that addressed the measurements of minor atmospheric species, e.g., excited-state N_2 (Garner and Dao, 1995), aurorally excited species (Collins et al., 1997), and metastable He (Gerrard et al., 1997). In contrast, the technique discussed in this paper is based on resonant Raman scattering and targets the measurements of temperature by probing a major atmospheric component.

We have recently suggested a Raman lidar experiment for in situ measurement of atomic oxygen density and temperature (Sharma and Dao, 2005). This experiment determines the O density and temperature in the immediate vicinity of the spacecraft in the lower thermosphere. In this article we extend this experiment to remote sensing from the ground. In the experiment proposed here, we would resonantly excite the $O(^3P_2)\rightarrow(^1D_2)$ and $O(^3P_1)\rightarrow(^1D_2)$ transition by two lasers tuned to 630.0304 and 636.3776 nm, respectively. While resonant Raman lidar has been studied and discussed for lidar measurements of atmospheric molecules (Hochenbleicher et al., 1976; Measures, 1984), resonant Raman for atoms has not been generally considered for lidar measurements. It is generally accepted that atoms has negligible Raman cross sections. The resonant Raman differential cross section of O, as shown later, is 10^{-29}–$10^{-26}\,cm^2\,sr^{-1}$—comparable to the molecular Raman differential cross section (Measures, 1984). The backscattered Raman signal for the laser tuned to 630.0304 [636.3776] nm is detected at 636.3776 (anti-Stokes transition) [630.0304 (Stokes transition)] nm, while the atom undergoes transition $^1D_2\rightarrow{}^3P_1$ ($^1D_2\rightarrow{}^3P_2$), giving a signal proportional to the $^3P_2$ [$^3P_1$] density in a given space time interval. Up to about 300 km altitude the rate of decay of the $O(^1D)$ atoms is dominated by collisions with N_2 and O_2. The scattering cross section up to these altitudes is therefore inversely proportional to the square of the density of N_2 and O_2. The ratio of the Stokes and anti-Stokes signal however depends only on the ratio of the densities of the two fine structure levels, $[O(^3P_2)]/[O(^3P_1)]$. Up to at least 350 km altitude, these two fine-structure levels are in thermodynamic equilibrium (Sharma et al., 1994), the ratio of the densities of the two fine structure levels gives the local temperature T, using the relation $[O(^3P_2)]/[O(^3P_1)] = (5/3)\exp(227.7/T)$ where 227.7 K is the spacing between the two levels (Fig. 1). For altitudes greater than about 300 km, when the $O(^1D)$ atoms decay mostly by emission of a photon, and the fine structure levels are still in thermodynamic equilibrium, the Stokes and anti-Stokes backscattered Raman signals give us the local temperature as well as the atomic oxygen density.

The technique described in this paper relies on the moderate differential cross section for resonant Raman scattering in the region above 90 km, where the spectral line shape is dominated by Doppler broadening. We begin by calculating the resonant cross section for the two Raman transitions. Our discussion of the principles of temperature measurement is followed by an assessment of the technique's sensitivity and error analysis. As mentioned earlier,

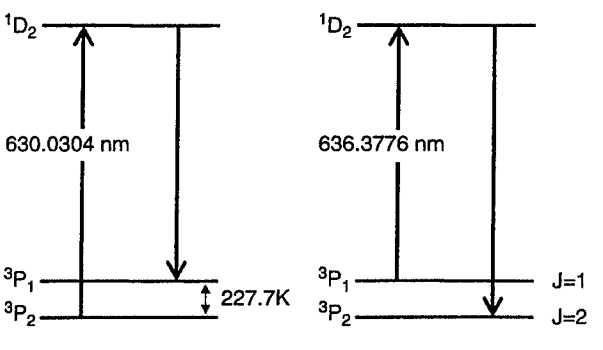

Fig. 1. Energy level diagram relevant to the Raman lidar. The transition from $^3P_2$ to $^1D_2$, with 630.0304 nm radiation, results in the Stokes line at 636.3776 nm. The transition from $^3P_2$ to $^1D_2$ with 636.3776 nm results in the anti-Stokes line at 630.0304 nm. The $^3P_0$ level, 98.8 K (68.7 cm^{-1}) from the $^3P_1$ level, is not shown because it is not involved in the resonant Raman excitation.

the temperature is derived from the relative signal strength of two transitions from ground states which are separated by an energy gap of 227.712 K. We then use a prototypical setup to project the performance of such a lidar system. The engineering aspects of implementing the lidar experiment are not dealt with in this paper.

Hochenbleicher et al. (1976) in a laboratory study for the applicability of resonance Raman scattering for remote analysis of air pollutant molecules "found that the influence of the absorption of the scattering gas can reduce the observed resonance Raman to normal Raman scattering levels." These authors were dealing with densities at sea level involving a large number of collisions in a radiative lifetime. To obtain measurable signals they had to deal with strong transitions (short radiative lifetime) so that a photon would be emitted before the excited state could be collisionally deactivated. Strong transition in turn induces self absorption, negating the advantage of resonance Raman cross sections. We are dealing with about six orders of magnitude smaller density at higher altitudes. With reduced collisional deactivation, we can use much weaker transitions. We can also deal with moderate transitions under the threshold of self absorption and take full advantage of enhanced resonance Raman scattering cross sections. At higher altitudes when the collisional deactivation of the excited state is negligible compared to the radiative deactivation the resonant Raman cross section becomes even larger. When the product of the dipole moment operators in the numerator is about the same as those involved in the radiative decay (Eq. (2)), as is the case under consideration, and the excited state decays only by emission, the resonant Raman cross section becomes independent of the strength of the transition to the intermediate state. The effects described here are, as the theory outlined below shows, are quite general and not due to any special set of circumstances.

2. Raman scattering cross section

The differential cross section for Raman scattering is given by (Kramers, 1964; Mizushima, 1970; Loudon, 1983)

$$\frac{d\sigma}{d\Omega}=\frac{\omega\omega_s^3}{c^4}\left|\sum_v\left(\frac{\langle f|(\boldsymbol{\varepsilon}_s\cdot\boldsymbol{\mu})|v\rangle\langle v|\boldsymbol{\varepsilon}\cdot\boldsymbol{\mu}|i\rangle}{(E_v-E_i-\hbar\omega+i(\hbar\Gamma_v/2))}+\frac{\langle f|(\boldsymbol{\varepsilon}\cdot\boldsymbol{\mu})|v\rangle\langle v|\boldsymbol{\varepsilon}_s\cdot\boldsymbol{\mu}|i\rangle}{(E_v-E_f+\hbar\omega)}\right)\right|^2, \quad (1)$$

where $\hbar\omega$ is the energy of the incident photon, $\hbar\omega_s$ the energy of the scattered photon, $|i\rangle$ the wavefunction of the initial state of the atom, $|v\rangle$ the wavefunction of the intermediate state of the atom, $|f\rangle$ the wavefunction of the final state of the atom, $\boldsymbol{\mu}$ the dipole moment vector operator, Γ_v the decay constant s^{-1} (radiative and nonradiative) of the intermediate atomic state, $\boldsymbol{\varepsilon}$ is the polarization (electric) vector of the incident photon, and $\boldsymbol{\varepsilon}_s$ the polarization (electric) vector of the scattered photon.

Since we are dealing with resonant Raman scattering for which $E_v = E_i + \hbar\omega$, the contribution of one intermediate state is expected to be much larger than that of any other intermediate state and in addition the contribution of the first term in Eq. (1) is expected to be much larger than that of the second term. We may therefore write

$$\frac{d\sigma}{d\Omega}=\frac{\omega\omega_s^3}{c^4}\left|\frac{\langle f|(\boldsymbol{\varepsilon}_s\cdot\boldsymbol{\mu})|v\rangle\langle v|\boldsymbol{\varepsilon}\cdot\boldsymbol{\mu}|i\rangle}{\hbar\Gamma_v/2}\right|^2. \quad (2)$$

Following Zare (1987), we write the following:

$$\boldsymbol{\varepsilon}\cdot\boldsymbol{\mu}=\left(\frac{4\pi}{3}\right)^{1/2}\mu\sum_{M=-1}^{M=+1}\varepsilon_M^* Y_{1M}(\Omega_\mu) \quad (3)$$

and

$$\boldsymbol{\varepsilon}_s\cdot\boldsymbol{\mu}=\left(\frac{4\pi}{3}\right)^{1/2}\mu\sum_{m=-1}^{m=+1}\varepsilon_{sm} Y_{1m}^*(\Omega_\mu), \quad (4)$$

where μ_0 (ε_0), μ_{-1} (ε_{-1}), μ_1 (ε_1) are the projections of the vector $\boldsymbol{\mu}$ ($\boldsymbol{\varepsilon}$) on the unit vectors along the z, $(1/2)^{1/2}(x-iy)$, and $-(1/2)^{1/2}(x+iy)$ axes, respectively. Radiation polarized along x-axis is obtained by the coherent (summing before taking absolute square) combination $(1/2)^{1/2}(\varepsilon_{-1}-\varepsilon_1)$ while that polarized along y-axis is represented coherently by the combination $(i/(2)^{1/2})(\varepsilon_{-1}+\varepsilon_1)$.

In our lidar experiment we take the incident beam traveling in the ε_{-1} direction with its polarization vector along the z-direction ($M=0$) (Sharma and Levin, 1973; Sharma, 2004). To distinguish the backscattered radiation from the Rayleigh scattered radiation, we will investigate only Stokes (red shifted) and anti-Stokes (blue shifted) Raman scattered photons. We are therefore restricted to the case where the initial and final states are different. The backscattered light can be polarized either in the z-direction ($m=0$) or the ε_1 direction ($m=1$). To determine atomic oxygen density and temperature we choose the initial and final states from the three multiplet levels of the ground state of

atomic oxygen ($O(^3P_J)$, $J = 0$, 1, and 2) and the only intermediate state is $O(^1D_2)$. This intermediate state is connected to all three J levels of the ground state by an electric quadrupole transition but is connected only to $J = 2$ at 630.0304 nm and $J = 1$ at 636.3776 nm by a magnetic dipole transition (http://physics.nist.gov/cgi-bin/ASD/lines1.pl) with Einstein A coefficient 0.00563 and 0.00182 s^{-1}, respectively (Table 1). Since the electric quadrupole transition probabilities for these two transitions are at least two orders of magnitudes smaller than the magnetic dipole transition probabilities, we will ignore the former. The electric quadrupole transition probability for the $O(^1D_2) \rightarrow O(^3P_0)$ transition at 639.1733 nm is $8.60 \times 10^{-7}\,s^{-1}$—a number so small that we will ignore it and will not consider the transitions from or to the $O(^3P_0)$ level further.

The Einstein A coefficient for the emission of a photon with a given direction of polarization for the $O(^1D_2) \rightarrow O(^3P_J)$ is given by (in Gaussian units)

$$A(^1D_2 \rightarrow {}^3P_J) = \frac{4\omega^3}{3\hbar c^3}\left(\frac{2J+1}{5}\right)|\langle {}^3P_J||\mu^{\mathrm{mag}}||{}^1D_2\rangle|^2, \tag{5}$$

where the expression in the brackets is the reduced magnetic dipole moment matrix element.

The values of the reduced dipole matrix elements are

$$|\langle {}^3P_2||\mu^{\mathrm{mag}}||{}^1D_2\rangle| = |\langle {}^1D_2||\mu^{\mathrm{mag}}||{}^3P_2\rangle| = 6.70 \times 10^{-23} \tag{6}$$

and

$$|\langle {}^3P_1||\mu^{\mathrm{mag}}||{}^1D_2\rangle| = \left(\frac{5}{3}\right)^{1/2}|\langle {}^1D_2||\mu^{\mathrm{mag}}||{}^3P_1\rangle| = 3.87 \times 10^{-23}. \tag{7}$$

Using the Wigner–Eckart theorem we can write

$$\langle {}^3P_{J',m'}|(\boldsymbol{\varepsilon}_s \cdot \boldsymbol{\mu})|{}^1D_{2,m}\rangle\langle {}^1D_{2,m}|\varepsilon_0\mu_0|{}^3P_{J,m}\rangle = (-1)^M \varepsilon_0\varepsilon_{-M} C(J12; m0m)C(21J; m, M, m') \times \langle {}^3P_{J'}||\mu^{\mathrm{mag}}||{}^1D_2\rangle\langle {}^1D_2||\mu^{\mathrm{mag}}||{}^3P_J\rangle\delta_{m',m+M}, \tag{8}$$

where m, M, and m' are magnetic quantum numbers of the initial atomic state, scattered photon, and final atomic state, respectively. The Cs are Clebsch–Gordan coefficients and $\delta_{m',m+M}$ is a Kronecker delta. Substituting the relation

$$C(J12; m, 0, m)C(21J'; m, M, m+M) = (-1)^{J-m}\sum_f [5(2J'+1)]^{1/2} W(J11J'; 2f) \times C(11f; 0, M, M)C(JJ'f; m, -M-m, -M), \tag{9}$$

where W is a Racah coefficient, into Eq. (8) and inserting the result into Eq. (2) which upon averaging over the initial magnetic quantum numbers and summing over the final ones, gives

$$\frac{d\sigma}{d\Omega} = \frac{\omega\omega_s^3}{c^4}\left(\frac{2}{\hbar\Gamma_v}\right)^2 |\langle {}^3P_{J'}||\mu^{\mathrm{mag}}||{}^1D_2\rangle \times \langle {}^1D_2||\mu^{\mathrm{mag}}||{}^3P_J\rangle|^2 \times \sum_{f=1,2}\sum_{M=0,1}\left(\frac{5(2J'+1)}{2J+1}\right) \times W^2(J11J'; 2f)C^2(11f; 0, M, M). \tag{10}$$

M denotes the polarization vector of the scattered beam ($M = 0$ for scattering without change in the direction of polarization and $M = 1$ for scattering with change in the direction of polarization), f is the rank of the tensor mediating the scattering process.

The $O(^1D_2)$ state of atomic oxygen is rapidly quenched by O_2 and N_2; the recommended quenching coefficients, by the Sander et al. (2003) are $3.2\,(\pm 1.2) \times 10^{-11}\exp(70/T)\,cm^3\,s^{-1}$ and $1.8(\pm 1.2) \times 10^{-11}\exp(110/T)\,cm^3\,s^{-1}$; the value at 200 K being $4.5(\pm 1.2) \times 10^{-11}\,cm^3\,s^{-1}$ and $3.1(\pm 1.2) \times 10^{-11}\,cm^3\,s^{-1}$, respectively. Taking the density of O_2 and N_2 at 100 km altitude to be $1.6 \times 10^{12}\,cm^{-3}$ and $6.5 \times 10^{12}\,cm^{-3}$, respectively, one estimates the decay probability $\Gamma_v = 273.5\,s^{-1}$. Figs. 2 and 3 plot the densities of the major thermospheric species and temperature, respectively, as function of altitude (Hedin, 1991). Because of its dependence upon density, Γ_v decreases with altitude and therefore differential Raman scattering increases with altitude reaching a limiting value when $\Gamma_v = 0.00745\,s^{-1}$, the

Table 1
Spectroscopic parameters

Transition	Wavelength (nm)	Einstein coefficient (s^{-1}) $\times 10^3$ magnetic dipole moment	Einstein coefficient (s^{-1}) $\times 10^5$ electric quadrupole moment
$^1D_2 \rightarrow {}^3P_2$	630.0304	5.63	2.11
$^1D_2 \rightarrow {}^3P_1$	636.3776	1.82	0.339
$^1D_2 \rightarrow {}^3P_0$	639.1733	0.00	0.0860

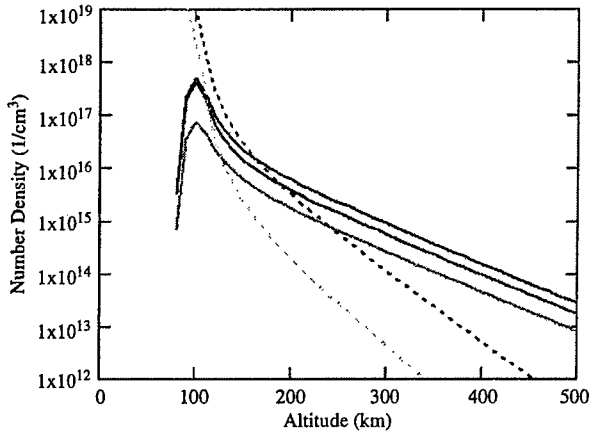

Fig. 2. Number density of atomic oxygen in $O(^3P_1)$ (red), $O(^3P_2)$ (blue), atomic oxygen total (black), molecular oxygen (dash green) and molecular nitrogen (dash black) as a function of altitude. The density of fine structure level $O(^3P_0)$ is not shown.

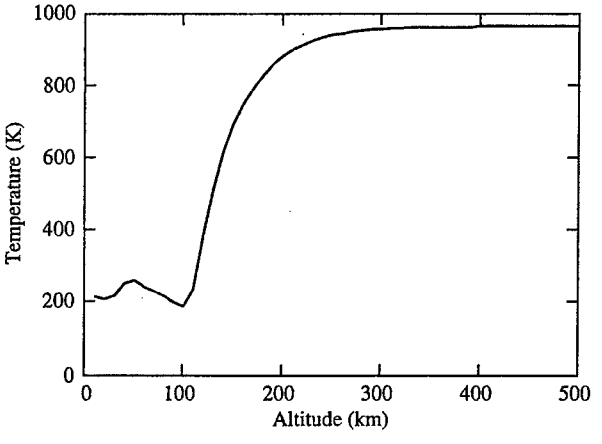

Fig. 3. Temperature as a function altitude.

spontaneous radiative decay constant. It is likely that the rate coefficient for quenching of $O(^1D_2)$ by ground state atomic oxygen $O(^3P)$, not found in the literature, is small because it would require dumping almost 2 eV of electronic energy into translational motion. We have therefore chosen to ignore it. The differential Raman scattering cross section ($cm^2\,sr^{-1}$) at 100 km altitude becomes

$$\left(\frac{d\sigma}{d\Omega}\right)_{100} = \frac{\omega\omega_s^3}{c^4}(4.81\times10^{49})|\langle{}^3P_{J'}||\mu^{mag}||{}^1D_2\rangle \times\langle{}^1D_2||\mu^{mag}||{}^3P_J\rangle|^2 \times\sum_{f=1,2}\sum_{M=0,1}\left(\frac{5(2J'+1)}{2J+1}\right)W^2(J11J';2f) \times C^2(11f;0,M,M). \quad (11)$$

For scattering without change in the polarization vector ($M=0$) and $J'\neq J$, the Racah coefficient and Clebsch–Gordan coefficients are both nonzero for only $f=2$; hence only $f=2$ contributes to the scattering process. The scattering, in other words, is mediated by a tensor of rank 2, and the expression for the scattering cross section at 100 km altitude becomes

$$\left(\frac{d\sigma}{d\Omega}\right)_{100,\parallel} = \frac{\omega\omega_s^3}{c^4}(4.81\times10^{49})|\langle{}^3P_{J'}||\mu^{mag}||{}^1D_2\rangle \times\langle{}^1D_2||\mu^{mag}||{}^3P_J\rangle|^2\times\left(\frac{5(2J'+1)}{2J+1}\right) \times W^2(J11J';22)C^2(112;0,0,0). \quad (12)$$

For $^3P_2\rightarrow{}^3P_1$ Stokes Raman transition ($J=2$, $J'=1$, $\omega=15,867.862\,cm^{-1}$, $\omega_s=15,709.597\,cm^{-1}$) without change in the direction of the polarization vector of the incident beam, the resonant Raman scattering cross section at 100 km altitude is $(d\sigma/d\Omega)_{100,2\rightarrow1,\parallel}=6.2\times10^{-22}\,cm^2\,sr^{-1}$.

For scattering with change in the polarization vector ($M=1$) and $J'J$, the Racah coefficient and Clebsch–Gordan coefficients are both nonzero for $f=1$ and 2; hence both $f=1$ and $f=2$ contributes to the scattering process. The expression for the scattering cross section (Eq. (11)) at 100 km altitude becomes

$$\left(\frac{d\sigma}{d\Omega}\right)_{100,\perp} = \frac{\omega\omega_s^3}{c^4}(4.81\times10^{49})|\langle{}^3P_{J'}||\mu^{mag}||{}^1D_2\rangle \times\langle{}^1D_2||\mu^{mag}||{}^3P_J\rangle|^2 \times\sum_{f=1,2}\left(\frac{5(2J'+1)}{2J+1}\right)W^2(J11J';2f) \times C^2(11f;0,1,1). \quad (13)$$

For the $^3P_2\rightarrow{}^3P_1$ Raman transition, substituting the values of Clebsch–Gordan and Racah coefficients, we get

$$\left(\frac{d\sigma}{d\Omega}\right)_{100,2\rightarrow1,\perp} = \frac{\omega\omega_s^3}{c^4}(4.81\times10^{49})\times0.1 \times|\langle{}^3P_1||\mu^{mag}||{}^1D_2\rangle \times\langle{}^1D_2||\mu^{mag}||{}^3P_2\rangle|^2 \quad (14)$$

giving $(d\sigma/d\Omega)_{100,2\rightarrow1,\perp}=2.8\times10^{-21}\,cm^2\,sr^{-1}$. The total cross section for Raman scattering 630.0304 nm photons into 636.3776 nm photons at 100 km altitude is therefore $(d\sigma/d\Omega)_{100,2\rightarrow1,\perp+\parallel}=3.4\times10^{-21}\,cm^2\,sr^{-1}$. When Doppler broadening is

included, the peak cross sections are respectively 1.6×10^{-27} and $1.9 \times 10^{-27}\,\mathrm{cm^2\,sr^{-1}}$.

Proceeding in a similar manner the differential cross section for the $^3P_1 \rightarrow {}^3P_2$ Raman transition, for Raman scattering 636.3776 nm photons into 630.0304 nm photons at 100 km altitude, is

$$\left(\frac{d\sigma}{d\Omega}\right)_{100,1\rightarrow 2,\perp+\parallel} = \left(\frac{d\sigma}{d\Omega}\right)_{100,1\rightarrow 2,\parallel} + \left(\frac{d\sigma}{d\Omega}\right)_{100,1\rightarrow 2,\perp}$$
$$= 1.0 \times 10^{-21} + 4.7 \times 10^{-21}$$
$$= 5.7 \times 10^{-21}\,\mathrm{cm^2\,sr^{-1}}.$$

3. Principles of temperature measurement

The method for deriving temperature from lidar Raman signals is best illustrated with the use of Fig. 1 which shows a partial energy level diagram, not drawn to scale, corresponding to the Raman transitions. The principles we applied are similar to that demonstrated by Gelbwachs on Fe atoms in the mesosphere (Gelbwachs 1994). In the diagram, the energy separation (in Kelvin units) between the $J = 2$ and the $J = 1$ levels is 227.712 K. The ratio of population at $J = 2$ level to $J = 1$ level in thermodynamic equilibrium at temperature T K is given by the Maxwell–Boltzmann relationship

$$\frac{n_2}{n_1} = (5/3)\exp(227.712/T). \tag{15}$$

With a temperature of 200 K at 100 km, the Boltzmann factor, right-hand side of Eq. (15), is estimated at 5.2. Because the population in the $J = 2$ level is 5.2 times greater than the $J = 1$ level and the Stokes (from $J = 2$ to $J = 1$). Since the Stokes differential cross section is about 0.6 times the anti-Stokes cross section, its volume backscatter coefficient is ~3 times higher than that of the anti-Stokes. Therefore if the oxygen atoms are in thermal equilibrium at the atmospheric temperature the ratio of Stokes to anti-Stokes backscatter signal can be used to measure the temperature.

The number of photons recorded by the lidar is given by the lidar equation as

$$S = \eta(E/h\nu)\Delta z \frac{A^2}{z^2} n_O \frac{d\sigma_O}{d\Omega}, \tag{16}$$

where η is the composite efficiency of the system, E is the transmitted laser pulse energy, $h\nu$ the photon energy, Δz the range gate, A the receiver area, z the altitude, n_0 the density of O atoms and $d\sigma_O/d\Omega$ the differential cross section for the Raman transition. The laser line width and wavelength stability are assumed to be less than the Doppler width (0.8 GHz at 200 K). The efficiency η includes the round trip atmospheric transmission, the transmission through the optics, and the quantum efficiency of the photomultiplier detector. The lidar equation is used to estimate the photon counts for the test cases. In comparing the signal for the anti-Stokes wavelength ($\lambda_{AS} = 636\,\mathrm{nm}: J = 1 \rightarrow J = 2$) to that for the Stokes wavelength ($\lambda_S = 630\,\mathrm{nm}: J = 2 \rightarrow J = 1$), one notes that all parameters in the lidar equation stay constant except photon energy, number density, differential cross section and atmospheric transmission. The ratio of Stokes to anti-Stokes signal is related to temperature as follows:

$$\frac{S_S}{S_{AS}} = \frac{\lambda_S}{\lambda_{AS}} \frac{d\sigma_{21}/d\Omega}{d\sigma_{12}/d\Omega} \frac{n_2}{n_1}. \tag{17}$$

In Eq. (17), the subscript S stands for the Stokes transition, AS for anti-Stokes, $d\sigma_{21}/d\Omega$ is the differential cross section for the Stokes transition from $J = 2$ to $J = 1$ level, and n_1 and n_2 are the number densities of O atoms in the $J = 1$ and $J = 2$ levels, respectively. Assuming that the laser pulse energy is independent of wavelength, the signal ratio under condition of thermodynamic equilibrium among the fine-structure levels of atomic oxygen is

$$\frac{S_S}{S_{AS}} = \frac{\lambda_S}{\lambda_{AS}} \frac{d\sigma_{21}/d\Omega}{d\sigma_{12}/d\Omega} \frac{g_2}{g_1} \exp\left(\frac{227.712\,\mathrm{K}}{T}\right). \tag{18}$$

In Eq. (18), g_J is the degeneracy of level $J(= 2J + 1)$ and 227.712 K is the energy separation in Kelvin units ($= \Delta E/k_B$). Using Eq. (11) for the differential cross section and noting that the number of scattered photons is inversely proportional to the cube of the wavelength, we can write

$$\frac{S_S}{S_{AS}} = \frac{\lambda_S^3}{\lambda_{AS}^3} \exp\left(\frac{227.712\,\mathrm{K}}{T}\right). \tag{19}$$

Near the altitude of 100 km, the temperature is related to the ratio of the Stokes and anti-Stokes signals R ($\equiv S_S/S_{AS}$) by

$$T = \frac{227.712\,\mathrm{K}}{\ln((\lambda_{AS}/\lambda_S)^3 R)}. \tag{20}$$

Differentiating the expression of T in Eq. (20) relative to R, we can show that the rate of temperature change is as follows:

$$\Delta T = \frac{T^2}{227.712\,\mathrm{K}} \frac{\Delta R}{R}. \tag{21}$$

The sensitivity factor, defined as the ratio of fractional change of T over fractional change of R, is ~1 for the conditions near the altitude of 100 km. If we assume that the change in R is dominated by the change in the $J = 1$ population or change in anti-Stokes signal, a 10% temperature detection limit requires measuring about 8% change of the anti-Stokes signal. That corresponds to a SNR of 10 or an anti-Stokes signal of 100 photon counts in the photon-limited regime and zero background noise. Eq. (21) predicts that the sensitivity factor will improve in the thermosphere because of higher temperatures as well as nearly equal populations of the $J = 1$ and $J = 2$ fine-structure levels.

A more general expression of the temperature error can be derived as follows. If one can neglect sky irradiance background and detector noise, the uncertainty in R will be dominated by the shot noise of photon counts and the temperature error is given by the expression

$$\frac{\Delta T}{T} = \frac{T}{227.712\,\mathrm{K}}\sqrt{(1/S_S) + (1/S_{AS})}. \tag{22}$$

According to Eq. (22), error in T is inversely proportional to the number of backscattered photons and hence to the square root of the integration time.

It should be noted again that the measurement of T is independent of atmospheric density. At lower altitudes when the collisional decay of $O(^1D)$ atoms is faster than the spontaneous radiative decay, both stokes and anti-stokes Raman cross sections are pressure and temperature dependent. The temperature dependence is due to the temperature dependence of quenching rate coefficients by collisions with O_2 and N_2 molecules. Since the pressure and temperature dependences cancel out in the ratio, the temperature measurement is insensitive to temperature and density change. That makes temperature remote sensing a robust technique in the upper mesosphere and lower thermosphere even though both temperature and atmospheric density vary considerably.

At higher altitudes when the decay of $O(^1D)$ atoms is due only to spontaneous radiative decay and the fine-structure levels of O are still in thermodynamic equilibrium, the backscattered signal no longer depends upon the local N_2 and O_2 density and this experiment can provide both atomic oxygen density and temperature. Density measurements are beyond the scope of this paper.

4. Error analysis of lidar measurements

The signal to noise ratio of lidar backscatter with the wavelength tuned in the Stokes resonance ($\lambda_S = 630$ nm:$J = 2 \rightarrow J = 1$) and the anti-Stokes resonance ($\lambda_{AS} = 636$ nm: $J = 1 \rightarrow J = 2$) is computed with the use of Eq. (16), the lidar equation. The assumptions about the transmitter, receiver, and other factors affecting the efficiency of the lidar are summarized in Table 2. To calculate the overall efficiency, the following values have been assumed: one-way atmospheric transmission of 0.65, telescope efficiency of 0.9, filter transmission of 0.65, and detection efficiency of photomultiplier detector of 0.20. In this first-order estimate of the SNR, errors in cross section due to laser tuning errors and laser line width errors are considered negligible. In the first test case, the signal strength for a ground-based lidar with characteristics as mentioned is displayed in Fig. 4. The atmospheric model used in the calculations is the Mass-Spectrometer-Incoherent-Scatter-Extended 90 (MSISE 90) (Hedin, 1991] with thermospheric temperature approaching 964 K.

To measure temperature in the lower thermosphere, the signals are integrated for 1 h. The estimated relative errors of the temperature profile are shown in Fig. 5. Measurements from a ground-based instrument with accuracy better than 30% are possible for altitudes between 120 and 250 km. This technique compliments the existing remote-sensing techniques, the upper limit of this temperature technique has been extended from the altitudes of minor metallic species, ~120 km, to the lower thermosphere near 300 km. This has the potential of providing unique data that addresses the modeling of satellite drag and the effects of space weather on the upper atmosphere.

Table 2
Lidar parameters used in the SNR estimates

Parameter	Ground lidar
Aperture diameter	3.5 m
Laser energy (J/pulse)	0.05
Repetition rate (Hz)	30
Range gate	3 km
Quantum efficiency of photon counting (PMT)	0.2
One way transmission	0.65
Optical efficiency:	
Interference filter	0.65
Telescope	0.9
Overall efficiency η	0.049

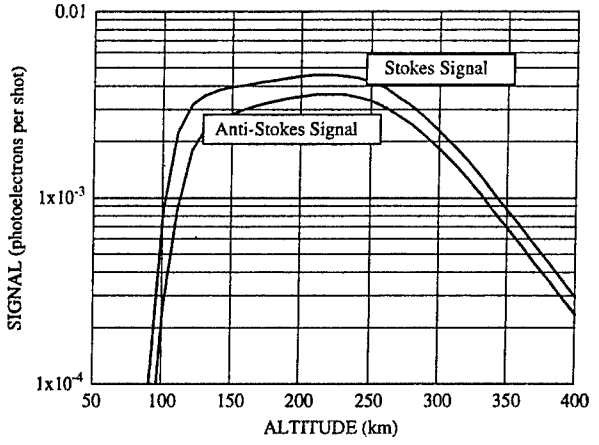

Fig. 4. Signal strength in photon counts per pulse as a function of altitude for a ground based lidar.

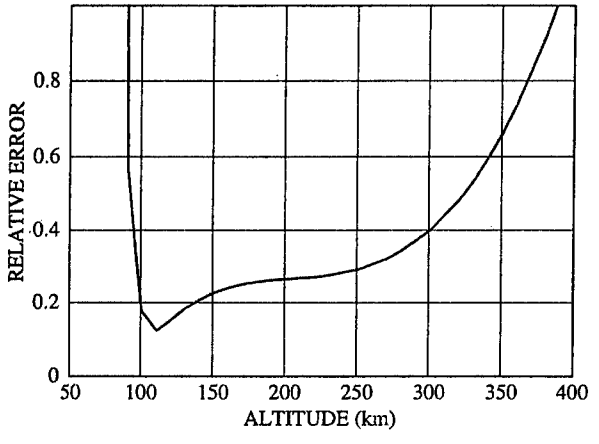

Fig. 5. Relative error in temperature for a ground-based lidar with signal integrated over 1 h. Table 1 lists the lidar parameters.

5. Summary

We have calculated the resonant cross sections for the Stokes and anti-Stokes atomic oxygen and introduced a new lidar technique for temperature measurement in the 90–290 km region. The lidar wavelengths are resonant with the anti-Stokes transition ($\lambda_{AS} = 636\,\text{nm}: J = 1 \rightarrow J = 2$) and the Stokes transition ($\lambda_S = 630\,\text{nm}: J = 2 \rightarrow J = 1$) for atomic oxygen. At 100 km, the temperature relative error is approximately equal to the error of the ratio of the anti-Stokes over Stokes signals. Based on the prototypical setup we project that a lidar can be built to routinely measure range-resolved temperature in the region where no alternative diagnostics exist. This system could be significant to the study of gravity waves, neutral density drag and space weather effects in the upper mesosphere and lower thermosphere.

Acknowledgment

The authors gratefully acknowledge instructive discussions with Dr. Steven M. Miller.

References

Collins, R.L., Lummerzheim, D., Smith, R.W., 1997. Analysis of lidar systems for profiling aurorally excited molecular species. Appled Optics 36, 24.

Gardner, C.S., 1989. Sodium resonance fluorescence LIDAR applications in atmospheric and astrononomy. Proceedings of the IEEE 77, 408.

Garner, R., Dao, P.D., 1995. Molecular nitrogen fluorescence lidar for remote sensing of the auroral ionosphere. Journal of Geophysical Research 100, 14131.

Gelbwachs, J.A., 1994. Iron Boltzmann factor LIDAR: proposed new remote-sensing technique for mesospheric temperature. Applied Optics 33 (30).

Gerrard, A.J., Kane, T.J., Meisel, D.D., Thayer, J.P., Kerr, R.B., 1997. Investigation of a resonant lidar for measurement of ionospheric metastable helium. Journal of Atmospheric and Solar-Terrestrial Physics 59, 16.

Hedin, A.E., 1991. Extension of the MSIS thermosphere model into the middle and lower thermosphere. Journal of Geophysical Research 96, 1159.

Hochenbleicher, J.G., Keifer, W., Brandmuller, J., 1976. A laboratory study for a resonance Raman lidar system. Applied Spectroscopy 5, 528.

Kramers, H.A., 1964. Quantum Mechanics. Dover Publications, Inc., New York.

Loudon, R., 1983. The Quantum Theory of Light. Clarendon Press, Oxford, UK.

Measures, R.M., 1984. Laser Remote Sensing. Wiley-Interscience, New York.

Mizushima, M., 1970. Quantum Mechanics of Atomic Spectra and Atomic Structure. W.A. Benjamin, Inc, New York.

Sander, S.P., et al., 2003. Chemical Kinetics and Photochemical Data for Use in Atmospheric Studies. JPL Publication No. 02-25.

Sharma, R.D., 2004. Raman scattering by ground-state atomic oxygen. Journal of Geophysical Research 109, A07303.

Sharma, R.D., Dao, P.D., 2005. In-situ measurement of atmospheric temperature and atomic oxygen density in the 90–150 km altitude range by a Raman lidar. Journal of Atmospheric and Solar-Terrestrial Physics 67, 1519.

Sharma, R.D., Levin, L.A., 1973. Polarization characteristics of Raman scattered radiation as a function of angle between incident and scattered beams. Journal of Chemical Physics 58, 1660.

Sharma, R.D., Roble, R.G., 2001. Impact of the new rate coefficients for O atom vibrational deactivation and photodissociation of NO on the temperature and density of the terrestrial atmosphere. Journal of Geophysical Research 10, 21,343.

Sharma, R.D., Roble, R.G., 2002. Cooling mechanisms of the planetary thermospheres: the key role of O atom vibrational relaxation of CO_2 and NO. ChemPhysChem 3, 841.

Sharma, R.D., Zygelman, B., von Esse, F., Dalgarno, A., 1994. On the relationship between the population of the fine structure levels of the ground electronic state of atomic oxygen and the translational temperature. Geophysical Research Letters 21, 1731.

von Zahn, U., Hoffner, J., 1996. Mesosphere temperature profiling by potassium LIDAR. Geophysical Research Letters 23, 141.

Zare, R.N., 1987. Angular Momentum; Understanding Spatial Aspects in Chemistry and Physics. Wiley, New York.

REPORT DOCUMENTATION PAGE

Form Approved
OMB No. 0704-0188

Public reporting burden for this collection of information is estimated to average 1 hour per response, including the time for reviewing instructions, searching existing data sources, gathering and maintaining the data needed, and completing and reviewing this collection of information. Send comments regarding this burden estimate or any other aspect of this collection of information, including suggestions for reducing this burden to Department of Defense, Washington Headquarters Services, Directorate for Information Operations and Reports (0704-0188), 1215 Jefferson Davis Highway, Suite 1204, Arlington, VA 22202-4302. Respondents should be aware that notwithstanding any other provision of law, no person shall be subject to any penalty for failing to comply with a collection of information if it does not display a currently valid OMB control number. **PLEASE DO NOT RETURN YOUR FORM TO THE ABOVE ADDRESS.**

1. REPORT DATE *(DD-MM-YYYY)*	2. REPORT TYPE	3. DATES COVERED *(From - To)*
04-01-2006	Reprint	

4. TITLE AND SUBTITLE
A Potential Remote-Sensing Technique for the Thermospheric Temperature with Ground-based Resonant Atomic Oxygen Raman Lidar

5a. CONTRACT NUMBER

5b. GRANT NUMBER

5c. PROGRAM ELEMENT NUMBER
62601F

6. AUTHOR(S)
Ramesh D. Sharma, Phan D. Dao

5d. PROJECT NUMBER
1010

5e. TASK NUMBER
SB

5f. WORK UNIT NUMBER
A1

7. PERFORMING ORGANIZATION NAME(S) AND ADDRESS(ES)
Air Force Research Laboratory/VSBYA
29 Randolph Road
Hanscom AFB MA 01731-3010

8. PERFORMING ORGANIZATION REPORT NUMBER
AFRL-VS-HA-TR-2006-1028

9. SPONSORING / MONITORING AGENCY NAME(S) AND ADDRESS(ES)

10. SPONSOR/MONITOR'S ACRONYM(S)

11. SPONSOR/MONITOR'S REPORT NUMBER(S)

12. DISTRIBUTION / AVAILABILITY STATEMENT
Approved for Public Release; Distribution Unlimited.

13. SUPPLEMENTARY NOTES
Reprinted from: Journal of Atmospheric and Solar-Terrestrial Physics, 2005 Elsevier Ltd. Doi: 10.1016/j.jastp.2005.10.001

14. ABSTRACT We propose a remote-sensing technique to measure temperature in the lower thermosphere with a resonant Raman lidar. A ground-based pulsed laser operating at 630.0304 (636.3776) nm excites $^3P_1$ ($^3P_2$) multiplet level of the ground electronic state of atomic oxygen in the atmosphere to the electronically excited state and the back-scattered photons at 636.3776 (630.0304)nrn, while the atom transitions to $^3P_1$ ($^3P_2$), are detected. Using the backscattering Rarnan cross sections calculated here we show: (1) For the range of altitudes in the lower thermosphere where the fine-structure multiplets of atomic oxygen are in thermodynamic equilibrium with the local translational temperature (LTE) and the electronically excited intermediate state $^1D_2$ remains relaxed primarily by collisions with N_2 and 0_2, the ratio of the backscattered signal can be used to obtain temperature. (2) Higher up, for the range of altitudes where the fine-structure multiplets of atomic oxygen are in LTE.and the electronically excited intermediate state $^1D_2$ is relaxed primarily by spontaneous emission of a photon, the Stokes and anti-Stokes backscattered signal can be used to obtain the atomic oxygen density and local temperature. (3) Still higher up, for the range of altitudes where the fine-structure multiplets of atomic oxygen are not in LTE and the electronically excited intermediate state is relaxed primarily by spontaneous emission of a photon, the Stokes and anti-Stokes backscattered signal **can** be used to obtain the density of the $^3P_2$ and $^3P_1$, multiplet levels of the ground electronic state of atomic oxygen. For a ground-based instrument a simulation with 3 km range gate is used to show that the relative error of temperature measurements from 100 to 250 km could be less than 30%. It is pointed out that this technique has the potential of providing unique data that addresses the modeling of satellite drag and the effects of space weather on the upper atmosphere. In addition, this technique may also permit the detection of the thickness of the temperature inversion layers as well as their temperature and density perturbations.

15. SUBJECT TERMS
Middle and upper atmosphere, Atomic oxygen density, Temperature, Resonant Rarnan scattering, Remote sensing

16. SECURITY CLASSIFICATION OF:			17. LIMITATION OF ABSTRACT	18. NUMBER OF PAGES	19a. NAME OF RESPONSIBLE PERSON
a. REPORT	b. ABSTRACT	c. THIS PAGE			Dr. Phan D. Dao
UNCLAS	UNCLAS	UNCLAS	SAR		19b. TELEPHONE NUMBER *(include area code)* 781-377-4944